Article

TRANSPARENT PROCESS

EMBO reports

GASZ and mitofusin-mediated mitochondrial functions are crucial for spermatogenesis

Jingjing Zhang[1], Qian Wang[1], Mingsong Wang[1], Manxi Jiang[2], Yongsheng Wang[1], Yun Sun[1], Junpeng Wang[1], Taorong Xie[3], Chao Tang[1], Nannan Tang[1], Huili Song[1], Di Cui[4], Ruihua Chao[1], Shuzhe Ding[4], Bing Ni[1], Xuejin Chen[2] & Yuan Wang[1,*]

Abstract

Nuage is an electron-dense cytoplasmic structure in germ cells that contains ribonucleoproteins and participates in piRNA biosynthesis. Despite the observation that clustered mitochondria are associated with a specific type of nuage called intermitochondrial cement (pi-body), the importance of mitochondrial functions in nuage formation and spermatogenesis is yet to be determined. We show that a germ cell-specific protein GASZ contains a functional mitochondrial targeting signal and is largely localized at mitochondria both endogenously in germ cells and in somatic cells when ectopically expressed. In addition, GASZ interacts with itself at the outer membrane of mitochondria and promotes mitofusion in a mitofusin/MFN-dependent manner. In mice, deletion of the mitochondrial targeting signal reveals that mitochondrial localization of GASZ is essential for nuage formation, mitochondrial clustering, transposon repression, and spermatogenesis. MFN1 deficiency also leads to defects in mitochondrial activity and male infertility. Our data thus reveal a requirement for GASZ and MFN-mediated mitofusion during spermatogenesis.

Keywords GASZ; MFN1; MFN2; mitofusion; spermatogenesis
Subject Categories Development & Differentiation; Membrane & Intracellular Transport
DOI 10.15252/embr.201540846 | Received 11 June 2015 | Revised 17 November 2015 | Accepted 19 November 2015 | Published online 28 December 2015
EMBO Reports (2016) 17: 220–234

Introduction

Mitochondria play important roles in various processes including ATP synthesis, production of reactive oxygen species (ROS), calcium signaling, and apoptosis [1–3]. The multifaceted functions of mitochondria are largely dependent on their dynamically changing structures [4]. For example, in somatic cells, the mitochondrial morphology changes primarily between a tubular type of fused active mitochondria and a spherical shape of fragmented quiescent arrangement to accommodate different energy requirements of cells and to maintain normal cellular homeostasis [1–3]. In adult testes, spermatogonia and leptotene spermatocytes contain orthodox mitochondria, whereas spermatocytes at later stages and spermatids mainly harbor the condensed form that is more efficient for ATP production [5,6]. Consistently, spermatogonia exhibit a higher glycolytic activity, while the spermatocytes and spermatids synthesize ATP mainly through mitochondria-mediated oxidative phosphorylation (OXPHOS) [5–8]. To date, the physiological significance underlying these changes in mitochondria in germ cell development remains unclear.

In most cells, mitochondria form an extended network that radiates from the nucleus, creating an interconnected system that supplies essential energy and metabolites [1–3,9]. In specialized cells, however, mitochondrial distribution is very different. One particular germinal granule that mitochondria are associated with in germ cells is nuage, which is an amorphous electron-dense structure in the cytoplasm without limiting membrane [10]. In embryonic gonocytes, postnatal spermatogonia, and spermatocytes, clustered mitochondria are found within a specific type of nuage (pi-body), which is therefore called intermitochondrial cement (IMC) as well [10,11]. Many germ cell-specific proteins are temporarily associated with this type of nuage, including GASZ, PIWI family members for piRNA biosynthesis (including MILI, MIWI, and MIWI2 in mice), MVH/VASA, TDRD1, and TDRD2 [12–18]. Loss of function of these proteins usually leads to disrupted formation of nuage, defective piRNA biosynthesis, upregulated transposon expression, and male infertility [12–18]. The nuage has thus been known for its roles in small RNA biosynthesis and the maintenance of genome integrity via repression of transposable elements by piRNAs [10,19,20]. It is unclear, however, how and why the mitochondria are clustered at IMC, how those germ cell-specific proteins are localized to IMC, and what role mitochondria may play during germ cell differentiation.

The heterogeneity in the distribution, activity, and morphology of mitochondria in various cell types is dynamically regulated

1 Shanghai Key Laboratory of Regulatory Biology, Institute of Biomedical Sciences and School of Life Sciences, East China Normal University, Shanghai, China
2 Department of Laboratory Animal Science, School of Medicine, Shanghai JiaoTong University, Shanghai, China
3 Key Laboratory of Nutrition and Metabolism, Institute for Nutritional Sciences, Shanghai Institutes for Biological Sciences, Chinese Academy of Sciences, Shanghai, China
4 Key Laboratory of Adolescent Health Assessment and Exercise Intervention, Ministry of Education, East China Normal University, Shanghai, China
*Corresponding author. Tel: +86 21 54345024; Fax: +86 21 54344922; E-mail: ywang@bio.ecnu.edu.cn

via fusion and fission events [1–3]. Mitochondria are double-membrane-bound organelles. Among proteins that participate in these processes, MFN1 and MFN2 are GTPases that are essential for outer membrane fusion, whereas DRP1 is the key enzyme that cooperates with FIS1 and MFF for mitochondrial fission [21–23]. The absolute reliance on mitochondrial fusion and fission has been highlighted in neuronal development. Mutations of *MFN2* is associated with Charcot–Marie–Tooth disease type 2A [24], an autosomal dominant neuropathy in human, and its deletion results in the reduction in dendritic outgrowth and spine formation in murine Purkinje cells as well [25]. It has been reported that *Fzo*, a *Drosophila* homolog for MFN, is mainly expressed in spermatids and plays a role at late meiosis II [26]. However, since mice with *MFN* null mutations are embryonic lethal [9], their functions in mammalian germ cell development have not been characterized. Recently, two reports demonstrated that MitoPLD, a phospholipase that facilities mitofusion, participates in nuage formation and piRNA biosynthesis during spermatogenesis [27,28]. Null mutation of *MitoPLD* in mice leads to the mislocalization of mitochondria and results in male infertility [27,28], thereby indicating a potential role of mitofusion during germ cell development.

GASZ is a germ cell-specific protein with four Ankyrin repeats/ANK, a sterile alpha motif/SAM, and a putative leucine zipper/ZIP [29]. Previous studies demonstrated that enforced expression of GASZ promoted $SSEA1^{+}$ germ cell derivation from both human and mouse embryonic stem cells (ESCs) [30]. Loss of function of GASZ leads to male infertility with defects in nuage formation and piRNA biosynthesis [17]. Yet the mechanisms by which GASZ affects these cellular function in germ cells have not been completely understood. We now report that GASZ contains C-terminal mitochondrial targeting sequences and that GASZ dimerizes at the outer membrane of mitochondria and interacts with MFNs to promote mitofusion. Additionally, the deletion of mitochondrial targeting sequences of GASZ or *MFN1* knockout leads to male infertility, demonstrating the absolute requirement for GASZ/MFN-mediated mitochondrial function in spermatogenesis.

Results

GASZ contains a mitochondrial localization signal

To explore the relationship of mitochondria to IMC formation, we searched for potential mitochondrial targeting sequences in proteins with known function or nuage localization in germ cells (Fig EV1A). According to the published reports, mitochondrial localization signals (MLS) generally lack acidic but are enriched in basic and hydrophobic amino acids, and they usually have the potential to fold into an amphiphilic α-helix [31,32]. We found that only three out of these proteins with known functions in germ cell development met these criteria and contained MLS (Fig EV1A). MitoPLD and TDRD2 were previously reported to contain MLS and localized at mitochondria [18,27,28]. The other one was murine GASZ that had a putative MLS at its C-terminus from amino acids 451 to 475 (Figs 1A and EV1A). The MLS of GASZ is also found in the orthologs from different species (Fig EV1B), including human and non-human primates, suggesting a functional conservation of GASZ–mitochondrial interactions during evolution.

To confirm the mitochondrial localization of GASZ, we examined its localization by subcellular fractionation assays. We observed that wild-type GASZ was co-enriched with MitoPLD in cytoplasmic and mitochondrial fractions (Fig 1B). As controls, nuclear protein NRF1 was largely restricted to the nucleus, whereas MVH, a known nuage protein without MLS, was found in the cytoplasm and mitochondria-free cytosol (Fig 1B). The mitochondrial localization of GASZ was further supported by direct fluorescence visualization. In this assay, we found that the localization of GFP completely overlapped with MitoTracker, but not with markers for other subcellular compartments when it was targeted at the N-terminus of GASZ (GFP-GASZ, Fig EV1C and D). In addition, GFP tagged with MLS alone from GASZ was directly recruited to mitochondria rather than its cytoplasmic localization on its own (Fig 1C). By contrast, mutated MLS (Phe/F to Pro/P mutation in MLS, GFP-F/P) or MLS with the deletion of its last four amino acids (ΔLQRK) failed to bring GFP to mitochondria (Fig 1C). These results, in large part, match those found in recent findings by Altshuller *et al* [33]. In common, we identified a functional MLS at the C-terminus of GASZ protein, and its mutation leads to the mislocalization of GASZ from mitochondria to the cytoplasm in somatic cells.

The mitochondrial localization of GASZ is critical for male reproduction

To further elucidate the role of mitochondrial localization of GASZ *in vivo*, we deleted its MLS through CAS9/CRISPR-based gene targeting technique (Fig EV2). Out of the eight mice that were born, five male mice contained different types of MLS mutations (Fig EV2B). One of them harbored mutated MLS on both alleles (with a single-base pair (bp) insertion on one allele and 2-bp deletion on the other), and this mouse was later proved infertile (Fig EV2B: #2). Another male mouse with mutated MLS on both alleles appeared to be reproductively normal (Fig EV2B: #5). However, we found that GFP-GASZ fusion protein containing this type of MLS mutation (#5: LK to Q) was localized at mitochondria in HeLa cells (Fig EV2E), suggesting that the alteration of leucine and lysine residues at the beginning of MLS had no influence on the subcellular localization and functions of GASZ.

We chose a female mouse as the founder for further investigation because the mutations (5-bp deletion or GTA insertion/2-bp deletion) started just before the beginning of MLS and in turn totally abolished the downstream mitochondrial targeting sequence (Fig EV2B: #6). In addition, an EcoRI site was disrupted, which could be used for genotyping to detect the mutated MLS (Fig EV2A–D: #6). We confirmed that GASZ with this type of MLS mutations expressed at a slightly reduced level in testes compared to wild-type controls and abolished the mitochondrial localization of GASZ both in germ cells at day 7 postnatal and in HeLa cells when ectopically introduced (Figs 2A and B, and EV2E). Interestingly, both MILI and MVH displayed a diffused pattern in the cytoplasm of $GASZ^{\Delta MLS/\Delta MLS}$ gonocytes at 16.5 days post-coitum (dpc) instead of perinuclear granular mitochondrial localization in wild-type controls (Fig 2A), demonstrating mislocalized IMC proteins upon GASZ MLS mutation.

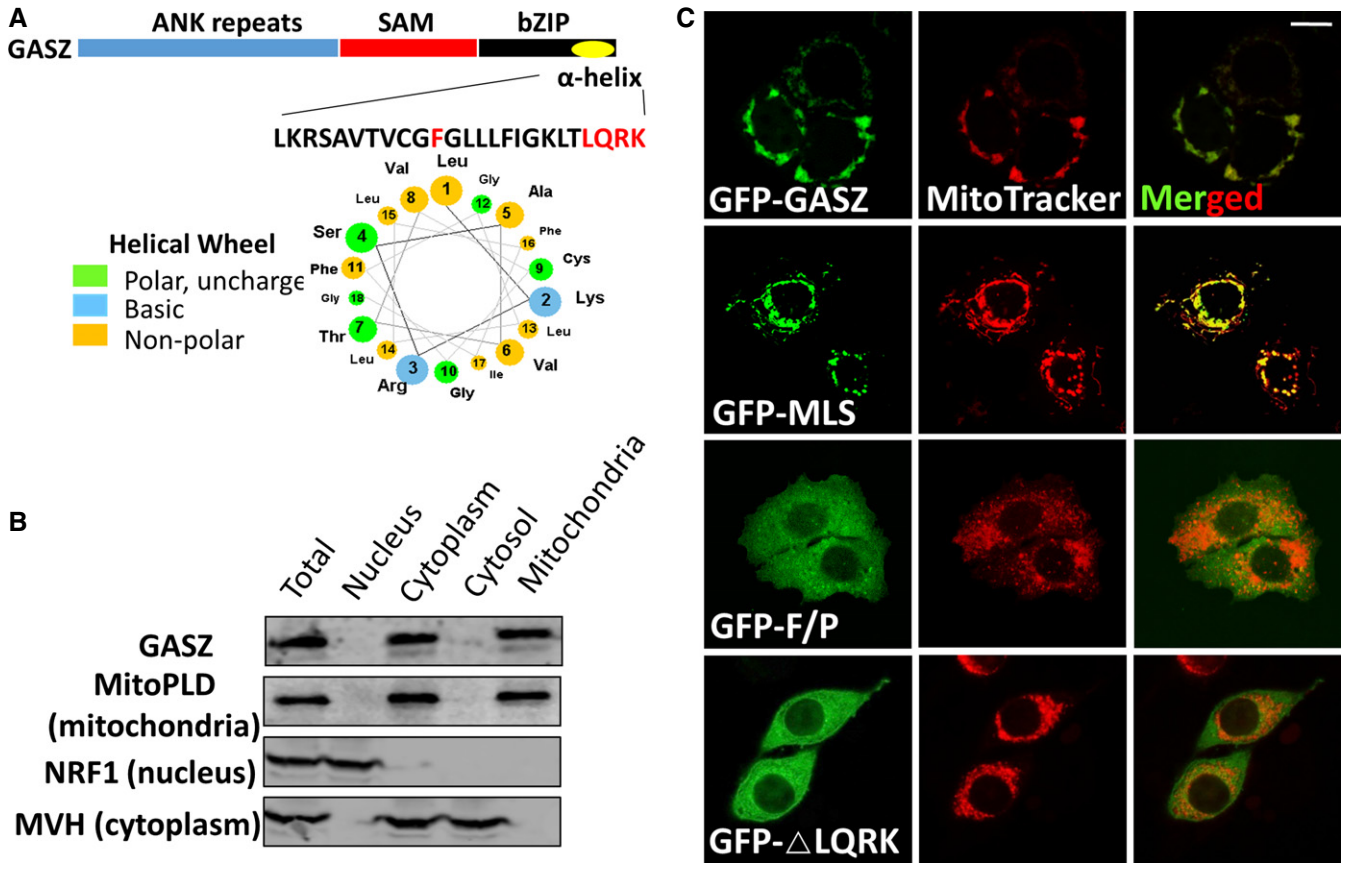

Figure 1. GASZ contains a mitochondrial localization signal.

A Predicated MLS localized at the C-terminus of GASZ and is enriched for hydrophobic amino acids that form a helical wheel.

B Subcellular fractionation and Western blots of 293T cells with ectopically expressed GASZ, NRF1, MVH, or MitoPLD.

C Localization of GFP fused with wild-type or mutant MLS of GASZ in HeLa cells. Mitochondrial localization was monitored by MitoTracker (Red) staining. Scale bars: 15 μm.

Female *GASZ*$^{\Delta MLS/\Delta MLS}$ mice exhibited no discernible phenotype and were fertile. By contrast, significant smaller testes were observed in adult male mice with MLS disruption at both alleles (Fig 2C). Although no obvious alterations were found in postnatal mutant mice at day 7, blocked development of *GASZ*$^{\Delta MLS/\Delta MLS}$ testes with fewer spermatocytes started to manifest by day 10 postnatal (Fig EV2G, P7 and P10). At P12, most of wild-type seminiferous tubules advanced to zygotene stage, in contrast to fewer than 20% of mutant tubules containing spermatocytes (Fig 2D). In addition, only spermatogonia and preleptotene spermatocytes were detected in *GASZ*$^{\Delta MLS/\Delta MLS}$ testes at day P14 (Fig 2D). By 8 weeks, few germ cells were left with a Sertoli-only phenotype in mice containing mutant MLS (Fig 2D).

As GASZ is associated with mitochondria at IMC in germ cells, we next examined the formation of IMC upon MLS disruption by transmission electron microscopy (EM). High electron-dense structures were clearly seen among clustered mitochondria in spermatogonia from wild-type neonatal mice (Fig 2E). By contrast, no discernible IMC was observed in *GASZ*$^{\Delta MLS/\Delta MLS}$ germ cells with a much lower degree of mitochondrial clustering as well (Fig 2E). In addition, consistent with the function of IMC as a site for the biosynthesis of piRNAs, which maintains transposon silencing and genomic stability in germ cells, the lack of IMC in turn led to a significant reduction in piRNA expression and an upregulation of transposon components including *IAP* and *Line1* in *GASZ*$^{\Delta MLS/\Delta MLS}$ testes (Figs 2F and EV3A). Taken together, these data demonstrate that mitochondrial localization of GASZ is essential for its function in nuage formation, transposon repression, and spermatogenesis.

GASZ interacts with itself at mitochondrial outer membrane

The experiments above demonstrated that mitochondrial localization of GASZ was required for spermatogenesis, so we next explored the potential functions of GASZ at mitochondria. According to bioinformatic prediction, GASZ possessed essential features as a tail-anchored membrane protein [34], with the same region of MLS as a transmembrane motif to target GASZ onto the mitochondrial outer surface (Figs 3A and EV4A). To validate this prediction, membrane-bound or soluble fractions were extracted from 293T cells with Na_2CO_3 treatment (which separated membrane-bound proteins from the soluble fraction) and examined for the existence of ectopically expressed GASZ by Western blots. We found that GASZ and

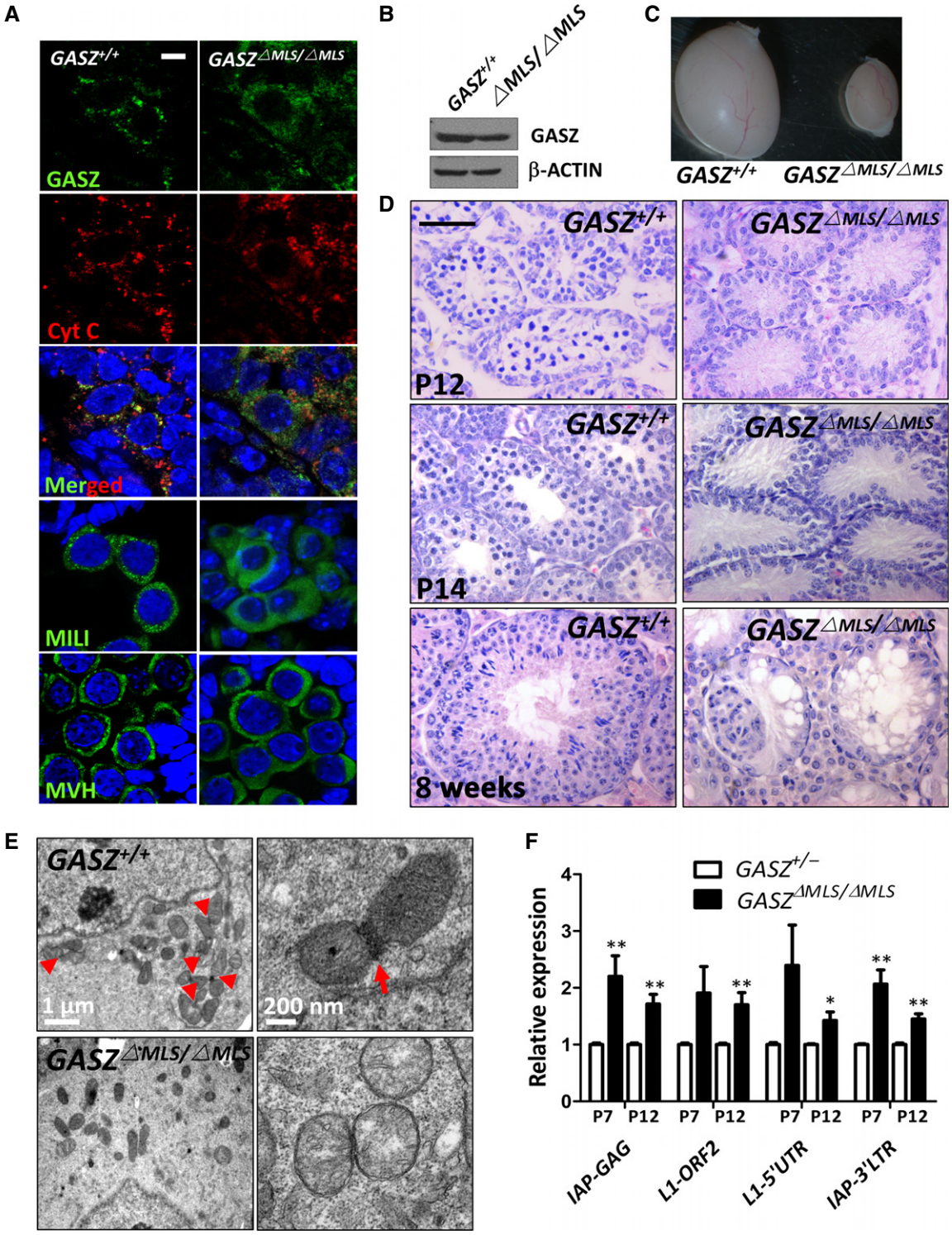

Figure 2. Mitochondrial localization of GASZ is essential for its function in male reproduction.

A IHF of GASZ and cytochrome c (Cyt c) of the testical sections from mice at day 7 postnatal, or MILI and MVH of gonad sections from wild-type embryos or embryos with MLS deletion at 16.5 dpc. Scale bar: 5 μm.

B Western blots of GASZ expression of testes at day 5 postnatal.

C Gross morphology of testes from adult mice at 3 months postnatal with mutated MLS compared to their wild-type littermates.

D Histological studies of testis sections from wild-type mice or mice with MLS deletion at different time points after birth. Scale bar: 50 μm.

E EM of testis sections from wild-type neonatal mice or mice with MLS mutation. Red arrows point to IMC among mitochondria.

F Expression of transposable elements analyzed by real-time RT–PCR on testes from wild-type mice or mice with mutated MLS at various time points after birth. Data were shown as mean (of expression from three biological replicates) ± 1 s.e.m. $n = 3$ for each genotype. $^{**}P < 0.01$. $^{*}P < 0.05$ (calculated by unpaired t-test).

MitoPLD were both enriched in the membrane-bound fraction, whereas SIRT3, a protein inside of mitochondria, largely existed in the soluble fraction (Fig 3B). This result was further confirmed by treating the extracted mitochondria with proteinase K and/or Triton X-100 (which permeabilized the mitochondrial membrane). Similar to outer membrane-bound MitoPLD [35], digestion of ectopically expressed GASZ by proteinase K alone was observed in the absence of Triton X-100 (Fig 3C). By contrast, SIRT3 and AIFM1, two proteins inside of mitochondria, were found degraded only in the presence of both proteinase K and Triton X-100 (Fig 3C). Therefore, these data clearly illustrate that GASZ indeed exists at the outer surface of mitochondria.

Since GASZ contains several protein-interacting domains including ANK and SAM, we then determined whether GASZ could associate with itself by GST pull-down assays. We observed that the GST-GASZ was indeed associated with FLAG-tagged GASZ in an *in vitro* binding reaction (Fig 3D), indicating that GASZ interacts with itself. In addition, ectopically transfected FLAG-tagged GASZ was pulled down with GFP-GASZ fusion protein from 293T cells (Fig 3E). The interaction was further supported by a Bimolecular Fluorescence Complementation (BiFC) assay, in which YFP was split into half and glowed only when these two halves were in proximity to each other [36]. Indeed, only weak fluorescence was detected when N-YFP and C-YFP were transfected into cells (Figs 3F and EV4B). By contrast, when the N- or C-terminal half of YFP was fused to GASZ separately and co-expressed, both flow cytometry and microscopy showed a much higher percentage of cells with brighter fluorescence (Figs 3F and EV4B). We further used co-immunoprecipitation (Co-IP) assays to determine the domains of GASZ that were required for its association and found that the interaction of GFP-GASZ with its FLAG-tagged deletion mutants was completely abolished in the absence of both SAM and ZIP motifs (Fig 3G). Taken together, these data demonstrate that GASZ interacts with itself at the mitochondrial outer membrane, likely through the SAM and ZIP domains.

GASZ affects mitochondrial dynamics and metabolism

GASZ interacts with itself at the outer membrane of mitochondria and thus may in turn bring mitochondria into proximity. Indeed, the aggregated mitochondria were observed when GASZ was ectopically expressed (Fig 4A). More importantly, aggregated and elongated mitochondria were clearly visible with transmission electron microscopy (EM) upon GASZ overexpression, and these were not seen when the MLS of GASZ was mutated (Fig 4B). In addition, we found that the formation of tubular mitochondria was increased when GASZ expression was enforced (Figs 4C and EV4C). This pro-mitofusion ability of GASZ was abolished either when MLS was mutated or when the domains (SAM and ZIP) required for its association were deleted (Figs 4C and EV4C). Mitochondrial dynamic was further monitored directly by visualization and quantification of dilution rate in a mitochondria-targeted photoactivable GFP (PAGFP) via time-lapsed confocal imaging. Normalized fluorescence intensity within designated region at photoactivation area was collected and plotted against time. Compared to control HeLa cells or cells with MLS-mutated GASZ, faster decrease in PAGFP fluorescence within photoactivated mitochondria was observed when wild-type GASZ overexpressed (Figs 4D and EV4D), reflecting increased mitochondrial fusion rate by GASZ overexpression.

Due to technical challenges to directly monitor the mitochondrial dynamics in primarily cultured gonocytes or in testes *in vivo*, we investigated whether GASZ affected mitofusion in germ cells using an immortalized spermatogonia cell line, C18-4, which was established by stable transfection of SV40 large-T antigen into A-type spermatogonial stem cells (SSC) [37]. Similar to somatic cells, ectopic expression of GASZ significantly enhanced the percentage of SSCs harboring tubular mitochondria (Figs 4E and EV4E). In addition, we observed an increased copy number of mitochondrial DNA (mtDNA) from $GASZ^{\Delta MLS/\Delta MLS}$ testes at day 14 postnatal (Fig 4F). Consistently, significantly higher activities of mtDNA-contributed respiratory enzyme complex including COX (cytochrome c oxidase in mitochondrial electron transport chain complex IV) and NADH dehydrogenase (a component of complex I) [25,38] were detected in $GASZ^{\Delta MLS/\Delta MLS}$ germ cells at days 10 and 14 postnatal, whereas the staining of SDH (succinate dehydrogenase in complex II), an enzyme entirely encoded by the nuclear genome [25,38], was not obviously altered (Figs 4G and EV4F and G), reflecting that the mislocalization of GASZ in germ cells leads to an increased mitochondrial fission and a dysregulated mitochondrial metabolism.

GASZ promotes MFN-dependent mitochondrial fusion

Since GASZ does not contain any catalytic motifs to initiate mitofusion by itself, we explored whether GASZ interacted with any known enzymes that engaged in mitofusion. Indeed, we found that GASZ interacted with two key GTPases in mitochondrial fusion, MFN1 and MFN2, both *in vitro* in GST pull-down assays (Fig EV5A) and in Co-IP (Fig 5A) and in testes *in vivo* (Fig 5B). By contrast, no evidence of interaction of GASZ with MitoPLD (an outer membrane-bound phospholipase in mitofusion) or DRP1 (a GTPase in mitochondrial fission) was found (Fig EV5C and D). In addition, GASZ appeared to be associated with both MFN1 and MFN2 via its SAM and ZIP domains, and failed to interact with MFNs when these

Figure 3. GASZ interacts with itself at mitochondrial outer membrane.

A Mouse GASZ contained a putative transmembrane domain and a region outside of the mitochondria predicted by a bioinformatic software TMHMM.

B 293T cells with ectopically expressed proteins were extracted for soluble and membrane-bound fraction and examined by Western blots.

C Mitochondrial fraction from 293T cells ectopically expressing GASZ, MitoPLD, AIFM1, or SIRT3 was treated in the presence or absence of Triton X-100 and/or proteinase K and examined by Western blots.

D GST pull-down assay of GST-tagged GASZ with FLAG-GASZ produced from 293T cells.

E Co-IP assays of FLAG or GFP-tagged GASZ in 293T cells. Antibodies for Co-IP (IP) or Western blots (WB) were listed on the left.

F BiFC assays in which YFP was detected by flow cytometry in control 293T cells, or 293T cells co-expressing GASZ fused with the N- or C-terminal half of YFP. Ctrl: empty vector control.

G Co-IP assays of GFP-GASZ with various FLAG-tagged wild-type GASZ or its deletion mutants in 293T cells.

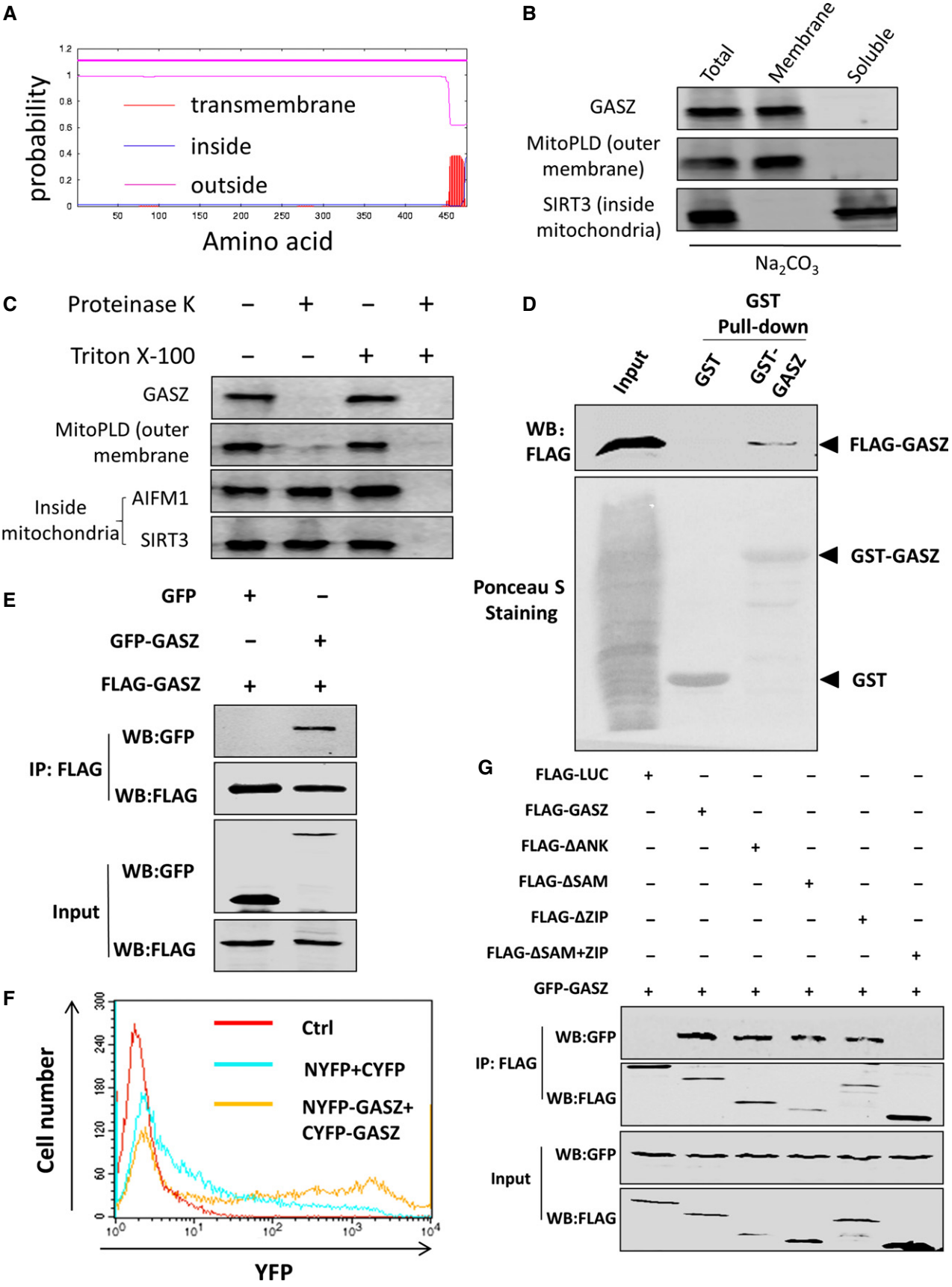

Figure 3.

domains were absent (Figs 5C and EV5E). Surprisingly, we observed that the MLS mutants of GASZ still interacted with MFNs (Figs 5C and EV5E), indicating that MLS mutations did not physically block the interaction of GASZ with MFNs.

To further investigate whether mitofusion enhanced by GASZ was functionally dependent on MFNs, we introduced a GASZ-expressing plasmid into wild-type mouse embryonic fibroblasts (MEFs), or MEFs with deletion of *MFN1*, *MFN2*, or both (Fig EV5F). We found that ectopically expressed GASZ promoted the formation of elongated mitochondria in wild-type MEFs, but was unable to increase the percentage of cells containing the tubular mitochondria in *MFN*-deficient MEFs (Figs 5D and EV5G). We further monitored the mitofusion directly between Su9-GFP- and COX4-DsRed-labeled mitochondria [9]. Upon induction by polyethylene glycol (PEG), GASZ significantly increased the percentage of fused mitochondria in wild-type MEFs, but failed to do so in the absence of MFN proteins (Figs 5E and EV5H). Taken together, these data demonstrate that GASZ promotes mitofusion in a MFN-dependent manner.

Mice with conditional *MFN1* deletion in germ cells are male infertile

So far, it is unknown whether MFN-mediated mitofusion is required for spermatogenesis. The mice with null mutation of *MFNs* failed to survive to midgestation [9]. To bypass the embryonic lethality, we used *MFN1* conditional knockout mice ($MFN1^{f/f}$) [25] and crossed them with a *MVH-Cre* line to obtain *MFN1* deletion specifically in germ cells (Fig EV6A), as Cre recombinase under the promoter of *MVH* started to be expressed only in gonocytes at 15.5 dpc [39]. $MFN1^{f/f}$*-Cre* mice were born at appropriate mendelian frequencies and appeared to be physiologically normal compared to their littermate controls. No obvious alteration in reproductive organs was observed in $MFN1^{f/+}$*-Cre* male mice either (data not shown).

We dissected the testes from $MFN1^{f/f}$*-Cre* and $MFN1^{+/+}$ mice after birth at different time points and found that the size of mutant testes was substantially reduced at 7 weeks compared to their wild-type littermates (Fig 6A). The defects in $MFN1^{f/f}$*-Cre* testes we observed were very similar to GASZ MLS-mutant mice. When leptotene/zygotene spermatocytes appeared at day 12 in wild-type testes, $MFN1^{f/f}$*-Cre* seminiferous tubules mainly contained spermatogonia (Fig EV6C). By day 14 after birth, most $MFN1^{+/+}$ tubules had advanced to mid-pachytene and zygotene stage, whereas only a few tubules in $MFN1^{f/f}$*-Cre* testical sections containing spermatocytes were detected (Fig 6B). At 6 weeks postnatal, few germ cells were seen in the seminiferous tubules in $MFN1^{f/f}$*-Cre* testes, along with a complete absence of sperms in epididymis (Fig 6B). In agreement with these findings, $MFN1^{f/f}$*-Cre* male mice were infertile, thereby demonstrating an essential requirement of MFN1 in spermatogenesis. Notably, *MFN1* deletion appeared to particularly affect the development of spermatocytes. No reduction in $PLZF^{+}$ spermatogonia was observed in $MFN1^{f/f}$*-Cre* testes by day 14 postnatal (Fig 6C).

Although no obvious alteration in the localization of GASZ, cytochrome c, MILI, and MVH in $MFN1^{f/f}$*-Cre* germ cells were observed via immunohistofluorescence (IHF) (Fig 6C), electron microscopy revealed two types of mitochondrial distribution in $MFN1^{f/f}$*-Cre* spermatogonia: One contained highly clustered mitochondria at one side of the cells, and another displayed evenly distributed mitochondria in the cytoplasm without perinuclear aggregation. Remarkably, mitochondria from $MFN1^{f/f}$*-Cre* spermatogonia in both cases were larger in diameter, round and swollen with vesiculated cristae inside (Fig 6D). Among clustered mitochondria, a thin layer of electron-dense IMC-like structure was observed, but appeared to be thinner and longer than the ones in wild-type cells (Fig 6D). Similar to GASZ MLS-mutant mice, $MFN1^{f/f}$*-Cre* testes at day 10 postnatal displayed increased activities of respiratory enzymes, COX and NADH dehydrogenase, with nuclear DNA-encoded SDH unaffected (Fig 6E), indicating a dysfunctional mitochondrial metabolism with a transient upregulation of mitochondrial fission due to *MFN1* null mutation. Taken together, these results reinforce the critical roles of mitochondria and MFN1-dependent mitofusion in the IMC formation and for the development of postnatal germ cells.

Discussion

In germ cells, structures with ribonucleoprotein aggregates known as IMC form among mitochondrial clusters [10,11]. Yet the understanding of the intricate interplay between mitochondria and germ cell development is still limiting and descriptive, especially with regard to the importance and underlying molecular mechanisms of

Figure 4. GASZ regulates mitochondrial fusion and metabolism.

A Mitochondria visualized by MitoTracker (Red) when wild-type GASZ or GASZ with MLS mutation was expressed in HeLa cells. Scale bar: 15 μm.

B EM on 293T cells with empty vector control (Ctrl), wild-type GASZ, or GASZ with F to P mutation in MLS. Scale bar: 1 μm. N: nucleus.

C Averaged percentage of HeLa cells (determined from 100 cells in each experiment) with different types of mitochondria determined by MitoTracker (Red) staining when transfected with GASZ, its SAM/ZIP deletion mutant, or GASZ with MLS mutation.

D HeLa cells transfected with COX4-DsRed, mito-PAGFP, and empty vector control, GASZ or GASZ with MLS mutation, followed by photoactivation of PAGFP. Representative images of PAGFP and DsRed were taken at 0, 10, and 20 min post-photoactivation. Scale bar: 10 μm. Insets show images with higher magnification. The averaged exponential decay constant (± s.e.m.) of normalized PAGFP fluorescence within the designated region (white circle) at photoactivation area over a period of 10 min was shown as a bar graph below. $n > 20$ cells for each group.

E Averaged percentage of C18-4 cells (determined from 100 cells in experiment) with different types of mitochondria determined by MitoTracker (Red) staining when transfected with Su9-GFP or GFP-GASZ.

F Real-time PCR analyses of mtDNA copy numbers on testes at different time points postnatal, relative to a single-copy gene, PECAM, encoded by nuclear DNA. $n = 5$ per genotype.

G Histochemistry of respiratory enzymes, COX, NADH, and SDH on testical sections from mice 10 days postnatal. Scale bar: 100 μm.

Data information: (C, E, F) Bars represent mean ± 1 s.e.m. calculated from three (C) or five (E, F) experiments or biological replicates. (C–F): $^{**}P < 0.01$ (calculated by unpaired *t*-test).

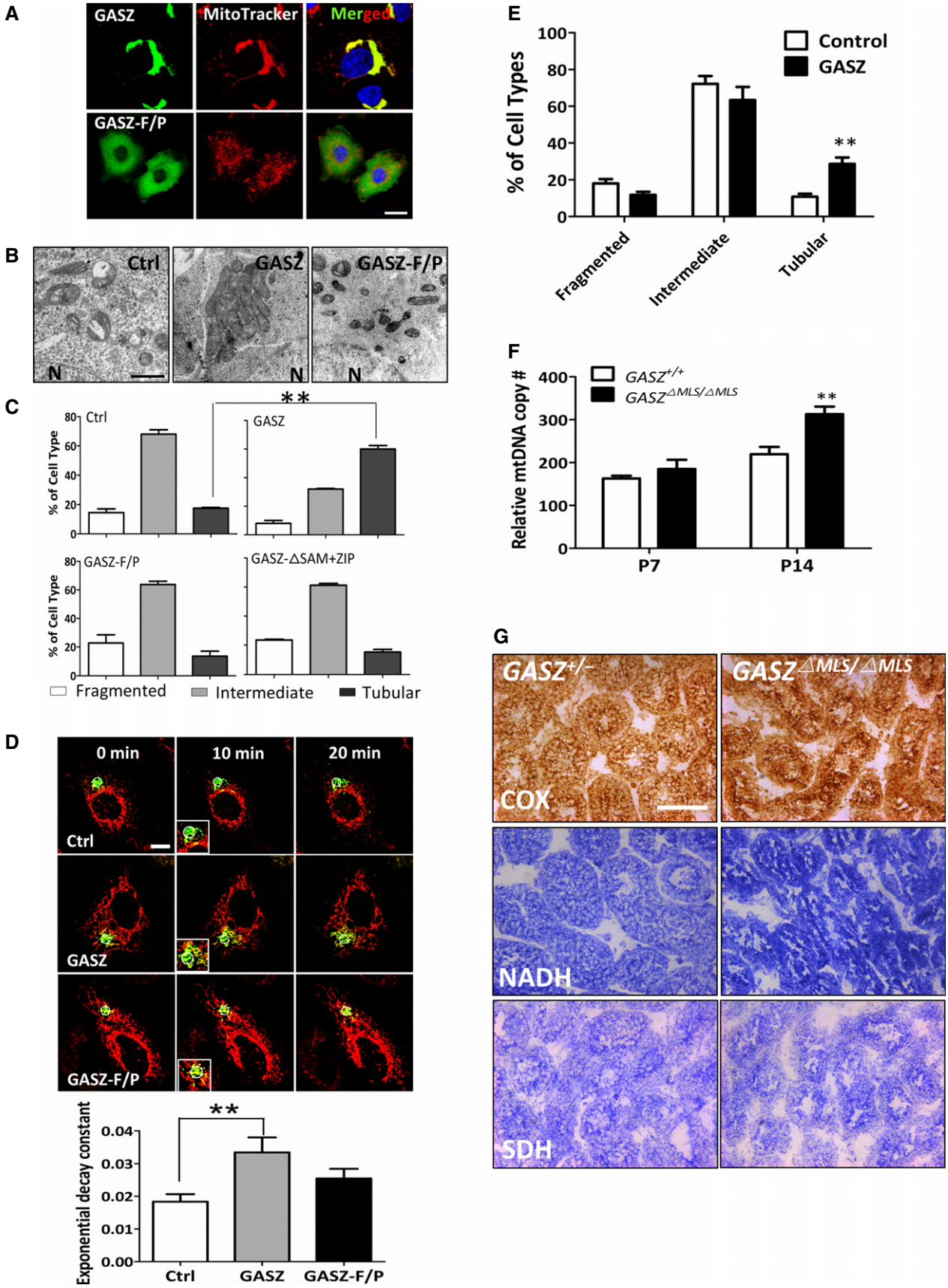
A
GASZ
MitoTracker
Merged
GASZ-F/P
B
Ctrl
GASZ
GASZ-F/P
N
C
Ctrl
GASZ
GASZ-F/P
GASZ-ΔSAM+ZIP
% of Cell Type
Fragmented
Intermediate
Tubular
D
0 min
10 min
20 min
Ctrl
GASZ
GASZ-F/P
Exponential decay constant
E
Control
GASZ
% of Cell Types
Fragmented
Intermediate
Tubular
F
GASZ+/+
GASZΔMLS/ΔMLS
Relative mtDNA copy #
P7
P14
G
GASZ+/−
GASZΔMLS/ΔMLS
COX
NADH
SDH

Figure 4.

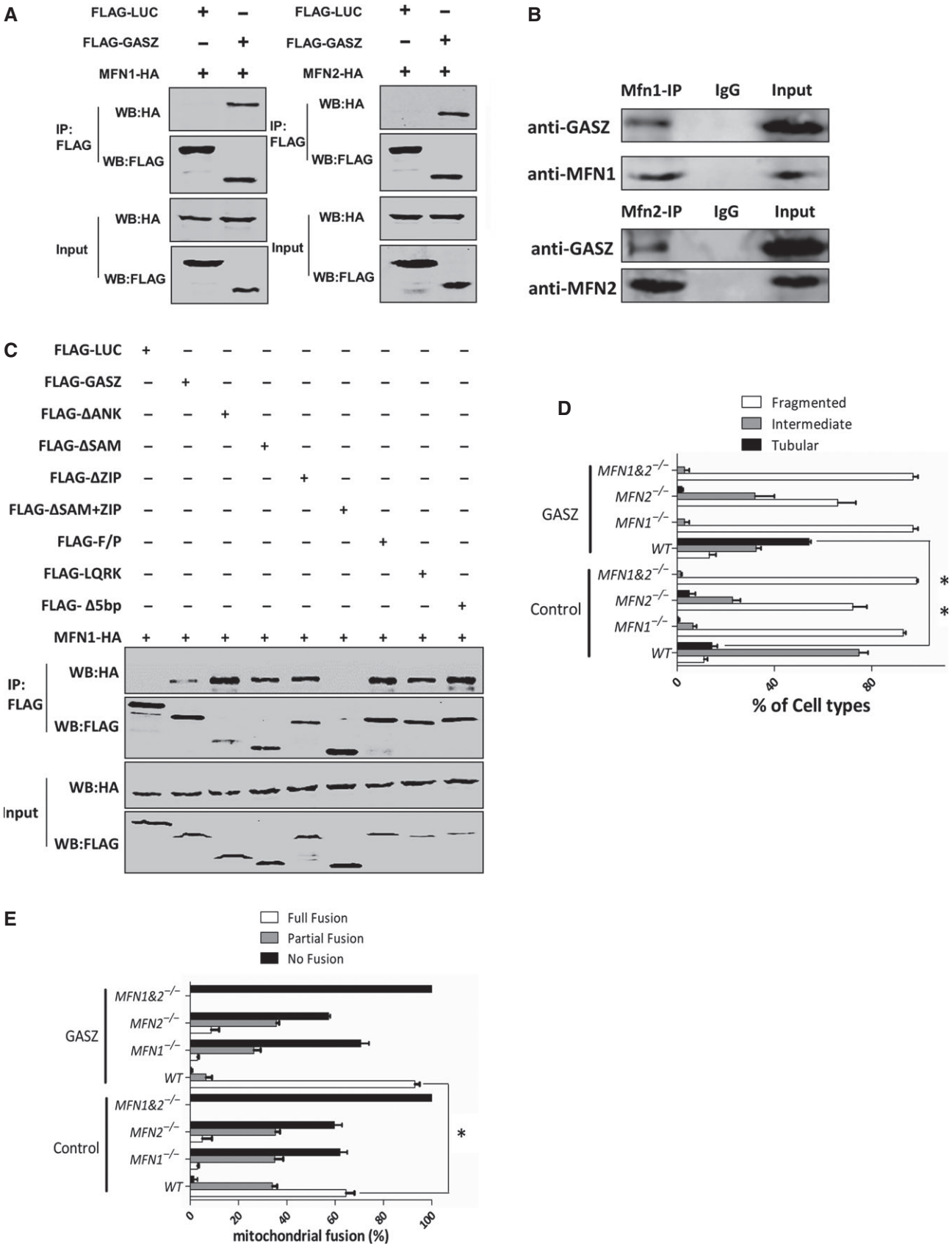

Figure 5.

Figure 5. GASZ promotes MFN-dependent mitochondrial fusion.

A, B Co-IP assays of ectopically expressed FLAG-GASZ and MFN-HA in 293T cells (A) or endogenous proteins of GASZ and MFNs from adult testes (B).

C Co-IP assays of HA-tagged MFN1 with various FLAG-tagged wild-type GASZ, its domain deletion mutants, or GASZ with MLS mutations in 293T cells.

D Averaged percentage of MEFs with different types of mitochondria were determined according to the mitochondrial morphology by MitoTracker (Red) staining in wild-type MEFs, or MEFs containing *MFN* null mutations transfected with empty vector control (Ctrl) or a GASZ-expressing plasmid.

E PEG fusion assays of Su9-GFP- and COX4-DsRed-labeled wild-type MEFs, or MEFs containing *MFN* null mutations transfected with empty vector control (Ctrl) or a GASZ-expressing plasmid. Bar graph represents averaged percentage of areas with different levels of mitochondrial fusion.

Data information: (D, E) Bars represent averaged percentage ± 1 s.e.m. calculated from 100 randomly chosen cells (D) or areas (E) for each assay in three independent experiments. $*P < 0.05$. $**P < 0.01$ (calculated by unpaired *t*-test).

mitochondria in IMC formation and spermatogenesis. So far, most *in vivo* experiments have focused on removing one component from nuage by loss-of-function assays, and thus, reproductive defects caused by which were usually due to the absence of the targeted proteins, but not their mislocalization. We found that a germ cell-specific protein GASZ formed dimers/oligomers at the outer membrane of mitochondria and promoted MFN-dependent mitochondrial aggregation and fusion. We thus took an alternative approach by specific deletion of MLS from GASZ to further discern the functional relevance of mitochondria and germ cell development in mice. Here, we demonstrated that mutation of MLS delocalized GASZ from mitochondria to the cytoplasm in germ cells and led to defects of IMC formation, abnormal mitochondrial metabolism, and male infertility. We further disturbed mitochondrial function in germ cells directly by conditional deletion of *MFN1*, a key GTPase in mitofusion, and this resulted in male infertility as well. Therefore, our results reveal a critical requirement of GASZ/MFN-mediated mitochondrial functions in germ cell development. Specifically, we propose that the roles of GASZ/MFN1 in these aspects are likely to be multifold.

Firstly, IMC is enriched with small RNAs (including microRNAs and piRNAs) and RNA-binding proteins (including MVH, an ATP-dependent RNA helicase, and PIWI family proteins in piRNA biosynthesis) [10]. GASZ may act as a central scaffold protein to recruit these germ cell-specific factors into close proximity at mitochondria at IMC. To support this hypothesis, multiple nuage-associated proteins (including MIWI, DAZL, MVH, and TDRD1) have been previously identified as interacting partners for GASZ [17,30,33]. Unlike a reported GASZ-knockout study [17], GASZ and MILI proteins were still found in the $GASZ^{\Delta MLS/\Delta MLS}$ gonocytes with the MLS deletion, and both of them displayed a diffused pattern in the cytoplasm instead of a perinuclear granular localization at mitochondria in wild-type controls. No discernable IMC was formed in the $GASZ^{\Delta MLS/\Delta MLS}$ neonatal testes either. Consistently, expression of piRNAs was significantly decreased, whereas transposable elements repressed by piRNAs were upregulated in $GASZ^{\Delta MLS/\Delta MLS}$ testes, likely due to disturbed piRNA biosynthesis caused by mislocalized GASZ and MILI. In this case, mitochondria likely function as central anchorages for RNA processing machinery. Mislocalization of GASZ from the mitochondria is sufficient enough to disrupt the normal IMC formation in germ cells and leads to defects in piRNA biosynthesis. Although GASZ interacts with mitochondria-bound MFNs, localization of GASZ may not rely upon MFNs and likely precedes its interaction with MFNs at mitochondria. The dynamic or weak interactions between GASZ and MFNs may not be strong enough to stabilize GASZ with mutant MLS to the mitochondria with MFNs.

Secondly, self-association of GASZ and its interaction with MFNs juxtapose mitochondria into clusters and contribute to the formation of IMC. Clustered mitochondria may form a "trap" to temporarily engage multiple RNA-binding proteins to act in concert needed for small RNA biosynthesis. Notably, MLS mutation of GASZ resulted in reduced mitochondrial clustering and defects in IMC formation, which in turn led to defects in the silencing of transposable components in germ cells. According to our knowledge, most known proteins involved in mitochondrial dynamics are ubiquitously expressed in both germ cells and somatic cells. Yet the mitochondrial clustering is only observed in embryonic gonocytes, postnatal spermatogonia, and spermatocytes. This indicates that some other germ cell-specific factors may be needed to aggregate mitochondria into proximity at IMC. The role of GASZ is thus unique as so far it is the only protein that has been proved to be germ cell specific, directly targets, and dimerizes/oligomerizes at mitochondria in somatic cells. Interestingly, high sequence similarity of MLS and the transmembrane motif in GASZ exists among different species, thereby suggesting an important functional conservation of GASZ at mitochondria in spermatogenesis during evolution.

Thirdly, GASZ-induced juxtaposition of mitochondria at IMC may provide the energy required for ATP-powered small RNA processing and germ cell maturation. It is known that dynamic mitochondrial fusion and fission act to allow cooperation between mitochondria, thereby maintaining their proper distribution, mtDNA stability, and energy requirement [1–3]. Since GASZ is not an enzyme that directly catalyzes mitofusion, it may functionally depend upon MFNs or other undefined cofactors in regulating mitochondrial activities. It is plausible that GASZ, together with MFNs, modulates the morphology and dynamics of mitochondria and in turn regulates the energy production of mitochondria for the surrounding RNA processing machinery in germ cells. In agreement with this notion, dysfunctional mitochondrial metabolism was observed in both *GASZ*- and *MFN1*-mutant testes, reflecting dysregulated mitochondrial dynamics in these mutant germ cells, and this may in turn lead to impaired germ cell maturation during spermatogenesis. As previously reported, the morphology, localization, and metabolism of testicular mitochondria change markedly during spermatogenesis, and the energy supply of differentiated spermatocytes relies primarily on mitochondrial metabolism [5,6]. Notably, although mitochondrial clustering or morphology appeared to be abnormal in the spermatogonia from neonatal mice, *GASZ* or *MFN1* mutations did not appear to affect $PLZF^{+}$ germline stem cells at early stages of spermatogenesis, but dramatically blocked the spermatocyte formation.

Although MFN1 and MitoPLD are both required for mitofusion, *MFN1* null mutant did not fully phenocopy the *MitoPLD* deficiency. Notably, no IMC was formed in $MitoPLD^{-/-}$ germ cells and mitochondria were mislocalized to the centrosome [27,28]. By contrast,

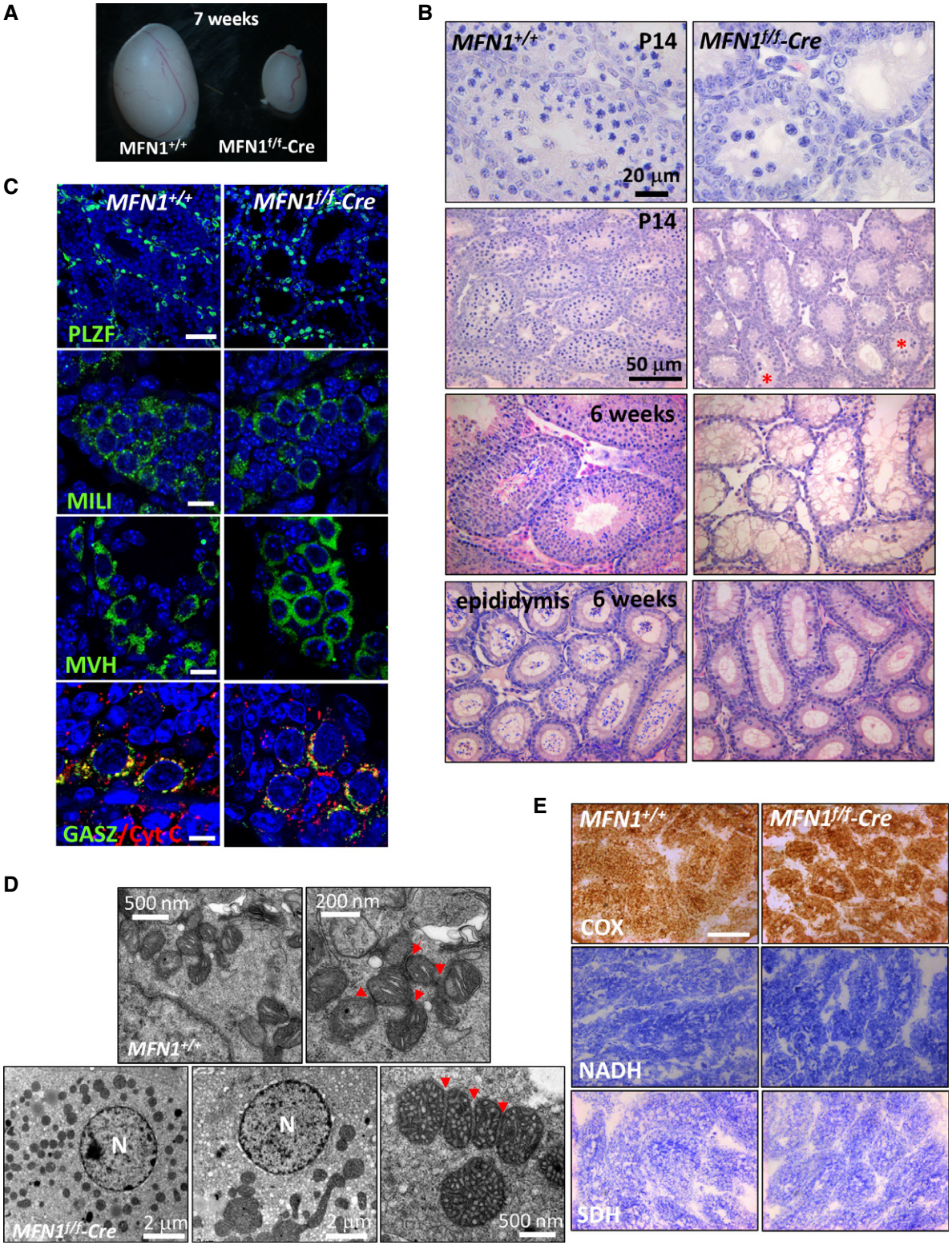

Figure 6. MFN1 deficiency led to male infertility.

A Gross morphology of testes from *MFN1$^{f/f}$-Cre* compared to their wild-type littermates.

B Histological studies of testis sections from wild-type mice or *MFN1$^{f/f}$-Cre* littermates at different time points postnatal. Red stars: tubules with spermatocytes.

C IHF of PLZF (day 14 postnatal), MILI, MVH, and GASZ/Cyt c (day 7) of testes sections. Scale bars for PLZF are 50 μm and 10 μm for others.

D EM of testical sections from wild-type neonatal mice or *MFN1$^{f/f}$-Cre* littermates. N: nucleus.

E Histochemistry of respiratory enzymes, COX, NADH, and SDH on testical sections from mice 10 days postnatal. Scale bar: 100 μm.

IMC was still observed in *MFN1* null spermatogonia, albeit appeared to be malformed compared to wild-type controls, reflecting a distinct functional contribution of MFN1-dependent mitofusion and mitochondrial metabolism in spermatogenesis. In addition, *MFN1* null mutation resulted in severe defects in mitochondrial morphology, evidenced by swollen and vesicular mitochondria. This phenotype is reminiscent of abnormalities observed in *MFN2*-deleted Purkinje cells [25]. Although both MFN1 and MFN2 were key GTPases involved in mitofusion, MFN2, but not MFN1, is required for proper mitochondrial functions of Purkinje cells [25], suggesting non-redundant roles of MFNs in neuronal development. It will be of great interest to investigate whether MFN1 and MFN2 are both required for spermatogenesis. Nevertheless, our data reveal an essential requirement of GASZ/MFN-mediated mitochondrial functions during spermatogenesis.

Materials and Methods

Plasmid construction

Genes used in this study were amplified from a cDNA library of mouse testis. *GASZ* cDNA was cloned into the vectors pEGFP-C1 (in which GFP was fused with N-terminus of GASZ), pEGFP-N2 (in which GFP was fused with C-terminus of GASZ), pcDNA3.1-CYFP, pcDNA3.1-NYFP, pGEX-4T-1 (in which GST was fused with N-terminus of GASZ), or pll3.7-3xFLAG-IRES-Hygro through XhoI and BamHI digestion. Domain deletion or MLS mutant for GASZ was constructed by PCR and QuickChange Site-Directed Mutagenesis Kit (Stratagene). For MitoPLD-HA and MFN-HA constructs, *MitoPLD, MFN1*, and *MFN2* cDNAs were cloned into pcDNA3.1-hygromycin in frame with a C-terminal HA tag. All primers used for cloning and PCR are listed in Table EV1.

Generation of GASZ MLS-mutant mice via CAS9/CRISPR

The CAS9 expressing vector pX260 and pGS3-T7-gRNA plasmid to express guide RNAs are kind gifts from Dr. Dali Li, East China Normal University (ECNU). pGS3-T7-gRNA vector was linearized by DraI and used as a template for *in vitro* transcription using *In Vitro* Transcription T7 Kit (Takara). To generate CAS9 mRNA, CAS9-expressing vector was linearized by NotI and transcribed into mRNA using the SP6 mMESSAGE mMACHINE Kit (Ambion). CAS9 mRNA and gRNAs were co-injected into zygotes of C57BL/6 mice. To identify the correct gene editing in progenies (all produced from breeding with C57BL/6 mice), tail genomic DNA was amplified by PCR and subjected to EcoRI digestion and/or sequencing. Guide RNA or genotyping primers are listed in Table EV1. All animal experimental procedures were conducted in accordance with the local Animal Welfare Act and Public Health Service Policy (consistent with the WMA Statement on Animal Use in Biomedical Research) and approved by the Committee of Animal Experimental Ethics at ECNU. Animals were housed at the facility with SPF condition and euthanized by carbon dioxide inhalation followed by cervical dislocation before dissection at various time points. The wild-type (or heterozygote) control and mutant littermates were chosen randomly according to their genotype. No blinding was done for animal experiments in this study.

Generation of conditional *MFN1* deletion in germ cells

Conditional *MFN1*-knockout mice were created previously [25]. Sperms harboring floxed *MFN1* allele were obtained from Mutant Mouse Regional Resource Center (MMRRC at UC Davis). Heterozygote $MFN1^{+/f}$ progenies were derived by intracytoplasmic injection of sperms into oocytes and maintained by crossing with C57BL/6 mice. $MFN1^{f/f}$ female mice were crossed with $MVH\text{-}Cre\text{-}MFN1^{+/f}$ male mice (*MVH-cre* mice from Model Animal Research Center at Nanjing University, China) to obtain targeted *MFN1* deletion in germ cells.

Cell culture, transfection, and viral infection

HeLa, 293T, $MFN1^{-/-}$, $MFN2^{-/-}$, and *MFN1&2*-double-knockout MEFs were maintained in DMEM with 10% fetal bovine serum (FBS, Gibco). For ectopic gene expression, 293T or HeLa cells (originally from ATCC) were transfected with plasmids using calcium phosphate or Lipofectamine®2000 (Invitrogen), respectively. MEFs were infected with retrovirus or lentivirus as previously described [30]. All cell lines were cleared from mycoplasma contamination by PCR with mycoplasma-specific primers.

Quantification of mitochondrial morphology and immunofluorescence (IF)

HeLa, C18-4, or MEFs cultured on gelatin-coated cover slips were transfected with expressing plasmids, incubated with 150 nM Mito-Tracker Red CMXRos (Invitrogen) at 37°C for 30 min, and fixed with 3.7% paraformaldehyde (PFA). Following permeabilization in ice-cold acetone or 1% Triton X-100, cells were directly analyzed or blotted with anti-FLAG antibody (Sigma) in 5% BSA/PBS and FITC-conjugated anti-mouse antibodies (Jackson ImmunoResearch). Mitochondrial morphology was visualized by Leica DM4000B. For each sample, 200 randomly chosen cells were counted and the percentage of different types of mitochondria-containing cells was calculated according to published reports [40].

PEG fusion assays and photoactivation assays

PEG fusion assays were performed according to the published protocols [9]. Briefly, 5×10^5 MEFs expressing mitochondria-targeted DsRed (COX4-DsRed) were cultured on cover slips overnight at the ratio of 1:1 with MEFs expressing mitochondria-targeted GFP (Su9-GFP). The cells were incubated in DMEM with 10% FBS containing 30 μg/ml cycloheximide (CHX) for 30 min and then treated with PEG1500 (Roche) for 2 min at room temperature. After washing with medium three times, the cells were cultured in media with 30 μg/ml CHX again for 5 h and fixed with 3.7% PFA for 15 min before being examined under confocal microscope (Leica TCS SP5) or Leica DM4000B. For photoactivation assay, the cells were grown in 2-well chambers and transfected with Mito-PAGFP (mitochondria-localized photoactivated GFP), COX4-DsRed, and empty control vector or GASZ-expressing plasmids via Lipofectamine®3000 (Invitrogen). Live cells were maintained at 37°C in assay solution (10 mM Hepes, 10 mM glucose, 3 mM KCl, 145 mM NaCl, 1.2 mM $CaCl_2$, 1.2 mM $MgCl_2$, pH 7.4), and images were captured with a FW1000 confocal

microscope (Olympus) using a 40 × 0.95 objective for time-lapse imaging and 60 × 1.2W objective for high-resolution imaging, respectively. Laser light at 405 nm was used for the photoactivation of PAGFP. DsRed was used to monitor the transfection efficiency and morphology of mitochondria in the same photoactivated cells. Normalized fluorescence intensity (dN = PAGFP-background/DsRed-background) within designated region at photoactivation area was collected every 10 s and plotted against time. Exponential decay constant λ ($dN/dt = -\lambda N$, t: time) of PAGFP was calculated. More than twenty cells for each group were randomly selected for quantitative analysis and imaging.

Transmission electron microscopy

EM was performed as described previously [27]. Briefly, samples were fixed with 2.5% EM-grade glutaraldehyde in 0.1 M PBS (pH 7.4) overnight and then fixed in 1% osmium tetroxide (OsO4) for 2 h at 4°C in the dark. After dehydration in a series of ethanol (30, 50, 70, 90%), the samples were treated in 45% ethanol and acetone for 15 min at 4°C and in 100% acetone three times. The samples were embedded in epoxy resin, processed into 60-nm sections, and counterstained with uranyl acetate and lead citrate before being examined under a Hitachi H7500 transmission electron microscope.

Subcellular fractionation and membrane extraction assays

The nuclear and cytoplasmic proteins or mitochondria and mitochondria-free cytosolic fractions of 293T cells were isolated using a Nuclear and Cytoplasmic Protein Extraction Kit or a Cell Mitochondria Isolation Kit (Beyotime) following the manufacturer's protocol. To determine whether target proteins were associated with mitochondrial membrane, the mitochondria-rich fractions were incubated in the presence or absence of 1% Triton X-100 with protease inhibitor cocktail (Sigma) in PBS at room temperature and/or following a treatment with 150 μg/ml proteinase K on ice for 15 min. For membrane extraction assay, the cells were harvested and subsequently incubated in 0.1 M Na_2CO_3, pH 11.5 on ice for 30 min, as described previously [41]. After centrifugation at 10,000 *g* for 30 min, the supernatants were collected as soluble proteins and the precipitates were enriched for the membrane-bound proteins. Target proteins were further examined by Western blots.

Western blots and Co-IP

Cells were harvested in lysis buffer (50 mM Tris, pH 7.4, 150 mM NaCl, 1 mM EDTA, 10% glycerol, and 1% Triton X-100 with protease inhibitor cocktail). The cleared supernatant was incubated with primary antibody, followed by treatment with Flag-M2 agarose (Sigma, A2220) or Protein A/G-agarose beads (Santa Cruz Biotech, SC-2003) to pull down antibody-interacting complex, which was subsequently separated by SDS–PAGE gel and transferred to nitrocellulose membranes. The membranes were blotted with primary antibodies, followed by secondary antibodies conjugated with IRDye®680 (LI-COR Biosciences, 926-68020) or IRDye®800CW (LI-COR Biosciences, 926-32211). The bands on the filter were observed by Odyssey infrared imaging system (LI-COR Biosciences). Primary antibodies used in this study were as follows: HA (Santa Cruz Biotech, SC-805); FLAG (Sigma, F7425); GFP (Santa Cruz Biotech, SC-8334); β-actin (Sigma, A5441); β-tubulin (Abmart, M30109); DRP1 (Cell Signaling, 8570), MVH (Abcam, ab13840); cytochrome c (Abcam, ab13575); MILI (Cell Signaling Technology, 5940); GASZ [42]; MFN1 and MFN2 (Abnova [43]).

GST pull-down assay

GST-GASZ fusion protein was induced by IPTG in bacteria at 33°C overnight, purified, and immobilized onto glutathione agarose beads. The protein–bead mixture was blocked with PBS containing 1% Triton X-100, 10 mg/ml BSA and incubated with 293T cell lysate containing FLAG-GASZ or MFN1/2-HA proteins for 3 h at 4°C. The bead-bound proteins were washed five times with PBS containing 1% Triton X-100 before being separated by SDS–PAGE and detected by Western blots.

Real-time RT–PCRs and PCRs

As previously described [44], total RNAs were extracted with TriZOL (Invitrogen) and cDNAs were synthesized using a PrimeScript® RT reagent kit (TaKaRa Biotechnology Co., Ltd.). For the determination of piRNA expression, reverse transcription was carried out using PrimeScript® RT Kit with gDNA Eraser (Takara) and piRNA-specific RT primers following the published protocols [45]. Genomic DNA and mtDNA were isolated from fresh mouse testes using PUREGENE DNA Purification kit (QIAGEN) and diluted to 5 ng/μl for the determination of mtDNA copy numbers relative to *PECAM* gene (a single-copy gene encoded by nuclear DNA) [46]. Quantitative real-time PCR was performed on Stratagene MX3000P instrument using SYBR Premix Ex TaqTM II (Takara). The mRNA and piRNA expression levels were normalized to β-actin or GAPDH and 5S rRNA, respectively. Primers used in this study are listed in Table EV1.

Histology and immunohistofluorescence (IHF)

Mouse testes were fixed in Bouin's fixative at 4°C overnight for staining with hematoxylin and eosin. For IHF, testes were fixed in 4% paraformaldehyde at 4°C overnight and embedded in paraffin. Antibodies used in this studies were as follows: guinea pig anti-GASZ [42], PLZF (Santa Cruz Biotech, SC-28319), MILI (Cell Signaling Technology), FLAG (Sigma), FITC-conjugated anti-guinea pig and FITC- or TRITC-conjugated anti-mouse, or anti-rabbit (Jackson ImmunoResearch, 706-095-148; 115-095-146, 115-025-146; 111-095-144 & 111-025-144). Nuclei were stained with 0.5 μg/ml 4′,6′-diamidino-2′-phenylindole (DAPI) for 5 min before being visualized by Leica TCS/SP5 confocal microscope and processed with Image-Pro Plus.

COX/NADH/SDH histochemistry

The activities of COX/NADH/SDH on testical sections were performed according to the published protocols [25,38] and online procedures from Washington University Neuromuscular Disease Center (http://neuromuscular.wustl.edu/index.html). Briefly, cryostat testical sections at 12 μm were prepared from fresh-frozen testical samples (n = 3 per genotyping group). Slides were incubated

for 40 min/60 min/30 min at 37°C with the COX/SDH/NADH reaction buffer, respectively, before visualization.

Statistical analysis and general method to avoid subjective bias

An online software TMHMM was used to predict MLS in germ cell-specific proteins (http://www.cbs.dtu.dk/services/TMHMM/), and ClustalX was used to compare the MLS conservation sequences among different species. For all experiments, three or more than three biological replicates have been performed, and the representative one (with others showing similar results) is shown in the figure for Western blot, Co-IP, HE, IF, IHF, and EM. All statistical analyses were performed using *F*-test (to estimate the variance within each group of data) and the unpaired *t*-test (for comparison between groups) with GraphPad Prism software. For all experiments, the criteria for inclusion/exclusion of samples were pre-established. Randomizing of sample allocation and measure as well as blinding of investigator was used when possible.

Expanded View for this article is available online.

Acknowledgements
We would like to thank Drs. Chuangui Wang and Dali Li at ECNU for plasmids containing FLAG-SIRT, FLAG-AIFM1, and pX260/gRNA constructs in CAS9/CRISPR system. We also thank Drs. David Chan (California Institute of Technology) for Su9-GFP and COX4-DsRed plasmids, Dr. Quan Chen (Institute of Physics, Chinese Academy of Sciences/CAS) for *MFN*-knockout mouse embryonic fibroblasts, Dr. Martin Dym at Georgetown University Medical Center for C18-4 cell line, and Dr. Martin Matzuk at Baylor College of Medicine for anti-GASZ antibody. We also thank Drs. Chen Xu at Tongji University, Degui Chen and Muofang Liu from CAS, Mitch Eddy from NIEHS, and Richard Mailman from Penn State College of Medicine for technical help in mouse work. This work was supported by grants from the Ministry of Science and Technology of China (2010CB945403 and 2014CB964800), the National Natural Science Foundation of China (31271589 and 30971522), the Science and Technology Commission of Shanghai Municipality (11DZ2260300 and 13JC1406402), China.

Author contributions
JZ, QW, MW, MJ, YW, YS, JW, TX, CT, NT, HS, DC, RC, and YW performed the experiments and analyzed the data. SD, BN, and XC contributed reagents and analysis tools. YW conceived and supervised the study. JZ, QW, and YW wrote manuscript.

Conflict of interest
The authors declare that they have no conflict of interest.

References

1. McBride HM, Neuspiel M, Wasiak S (2006) Mitochondria: more than just a powerhouse. *Curr Biol* 16: R551 – R560
2. Palmer CS, Osellame LD, Stojanovski D, Ryan MT (2011) The regulation of mitochondrial morphology: intricate mechanisms and dynamic machinery. *Cell Signal* 23: 1534 – 1545
3. Westermann B (2010) Mitochondrial fusion and fission in cell life and death. *Nat Rev Mol Cell Biol* 11: 872 – 884
4. Bereiter-Hahn J, Voth M (1994) Dynamics of mitochondria in living cells: shape changes, dislocations, fusion, and fission of mitochondria. *Microsc Res Tech* 27: 198 – 219
5. Ramalho-Santos J, Varum S, Amaral S, Mota PC, Sousa AP, Amaral A (2009) Mitochondrial functionality in reproduction: from gonads and gametes to embryos and embryonic stem cells. *Hum Reprod Update* 15: 553 – 572
6. Rato L, Alves MG, Socorro S, Duarte AI, Cavaco JE, Oliveira PF (2012) Metabolic regulation is important for spermatogenesis. *Nat Rev Urol* 9: 330 – 338
7. Bajpai M, Gupta G, Setty BS (1998) Changes in carbohydrate metabolism of testicular germ cells during meiosis in the rat. *Eur J Endocrinol* 138: 322 – 327
8. Boussouar F, Benahmed M (2004) Lactate and energy metabolism in male germ cells. *Trends Endocrinol Metab* 15: 345 – 350
9. Chen H, Detmer SA, Ewald AJ, Griffin EE, Fraser SE, Chan DC (2003) Mitofusins Mfn1 and Mfn2 coordinately regulate mitochondrial fusion and are essential for embryonic development. *J Cell Biol* 160: 189 – 200
10. Chuma S, Hosokawa M, Tanaka T, Nakatsuji N (2009) Ultrastructural characterization of spermatogenesis and its evolutionary conservation in the germline: germinal granules in mammals. *Mol Cell Endocrinol* 306: 17 – 23
11. Eddy EM (1974) Fine structural observations on the form and distribution of nuage in germ cells of the rat. *Anat Rec* 178: 731 – 757
12. Carmell MA, Girard A, van de Kant HJ, Bourc'his D, Bestor TH, de Rooij DG, Hannon GJ (2007) MIWI2 is essential for spermatogenesis and repression of transposons in the mouse male germline. *Dev Cell* 12: 503 – 514
13. Chuma S, Hosokawa M, Kitamura K, Kasai S, Fujioka M, Hiyoshi M, Takamune K, Noce T, Nakatsuji N (2006) Tdrd1/Mtr-1, a tudor-related gene, is essential for male germ-cell differentiation and nuage/germinal granule formation in mice. *Proc Natl Acad Sci USA* 103: 15894 – 15899
14. Grivna ST, Pyhtila B, Lin H (2006) MIWI associates with translational machinery and PIWI-interacting RNAs (piRNAs) in regulating spermatogenesis. *Proc Natl Acad Sci USA* 103: 13415 – 13420
15. Kuramochi-Miyagawa S, Kimura T, Ijiri TW, Isobe T, Asada N, Fujita Y, Ikawa M, Iwai N, Okabe M, Deng W *et al* (2004) Mili, a mammalian member of piwi family gene, is essential for spermatogenesis. *Development* 131: 839 – 849
16. Kuramochi-Miyagawa S, Watanabe T, Gotoh K, Takamatsu K, Chuma S, Kojima-Kita K, Shiromoto Y, Asada N, Toyoda A, Fujiyama A *et al* (2010) MVH in piRNA processing and gene silencing of retrotransposons. *Genes Dev* 24: 887 – 892
17. Ma L, Buchold GM, Greenbaum MP, Roy A, Burns KH, Zhu H, Han DY, Harris RA, Coarfa C, Gunaratne PH *et al* (2009) GASZ is essential for male meiosis and suppression of retrotransposon expression in the male germline. *PLoS Genet* 5: e1000635
18. Saxe JP, Chen M, Zhao H, Lin H (2013) Tdrkh is essential for spermatogenesis and participates in primary piRNA biogenesis in the germline. *EMBO J* 32: 1869 – 1885
19. Aravin AA, van der Heijden GW, Castaneda J, Vagin VV, Hannon GJ, Bortvin A (2009) Cytoplasmic compartmentalization of the fetal piRNA pathway in mice. *PLoS Genet* 5: e1000764
20. Grivna ST, Beyret E, Wang Z, Lin H (2006) A novel class of small RNAs in mouse spermatogenic cells. *Genes Dev* 20: 1709 – 1714
21. Bleazard W, McCaffery JM, King EJ, Bale S, Mozdy A, Tieu Q, Nunnari J, Shaw JM (1999) The dynamin-related GTPase Dnm1 regulates mitochondrial fission in yeast. *Nat Cell Biol* 1: 298 – 304

22. Labrousse AM, Zappaterra MD, Rube DA, van der Bliek AM (1999) *C. elegans* dynamin-related protein DRP-1 controls severing of the mitochondrial outer membrane. *Mol Cell* 4: 815 – 826
23. Santel A, Fuller MT (2001) Control of mitochondrial morphology by a human mitofusin. *J Cell Sci* 114: 867 – 874
24. Zuchner S, Mersiyanova IV, Muglia M, Bissar-Tadmouri N, Rochelle J, Dadali EL, Zappia M, Nelis E, Patitucci A, Senderek J *et al* (2004) Mutations in the mitochondrial GTPase mitofusin 2 cause Charcot-Marie-Tooth neuropathy type 2A. *Nat Genet* 36: 449 – 451
25. Chen H, McCaffery JM, Chan DC (2007) Mitochondrial fusion protects against neurodegeneration in the cerebellum. *Cell* 130: 548 – 562
26. Hales KG, Fuller MT (1997) Developmentally regulated mitochondrial fusion mediated by a conserved, novel, predicted GTPase. *Cell* 90: 121 – 129
27. Huang H, Gao Q, Peng X, Choi SY, Sarma K, Ren H, Morris AJ, Frohman MA (2011) piRNA-associated germline nuage formation and spermatogenesis require MitoPLD profusogenic mitochondrial-surface lipid signaling. *Dev Cell* 20: 376 – 387
28. Watanabe T, Chuma S, Yamamoto Y, Kuramochi-Miyagawa S, Totoki Y, Toyoda A, Hoki Y, Fujiyama A, Shibata T, Sado T *et al* (2011) MITOPLD is a mitochondrial protein essential for nuage formation and piRNA biogenesis in the mouse germline. *Dev Cell* 20: 364 – 375
29. Yan W, Rajkovic A, Viveiros MM, Burns KH, Eppig JJ, Matzuk MM (2002) Identification of Gasz, an evolutionarily conserved gene expressed exclusively in germ cells and encoding a protein with four ankyrin repeats, a sterile-alpha motif, and a basic leucine zipper. *Mol Endocrinol* 16: 1168 – 1184
30. Wang Q, Liu X, Tang N, Archambeault DR, Li J, Song H, Tang C, He B, Matzuk MM, Wang Y (2013) GASZ promotes germ cell derivation from embryonic stem cells. *Stem Cell Res* 11: 845 – 860
31. Roise D, Horvath SJ, Tomich JM, Richards JH, Schatz G (1986) A chemically synthesized pre-sequence of an imported mitochondrial protein can form an amphiphilic helix and perturb natural and artificial phospholipid bilayers. *EMBO J* 5: 1327 – 1334
32. von Heijne G (1986) Mitochondrial targeting sequences may form amphiphilic helices. *EMBO J* 5: 1335 – 1342
33. Altshuller Y, Gao Q, Frohman MA (2013) A C-terminal transmembrane anchor targets the nuage-localized spermatogenic protein Gasz to the mitochondrial surface. *ISRN Cell Biol* 2013: 707930
34. Rapaport D (2003) Finding the right organelle. Targeting signals in mitochondrial outer-membrane proteins. *EMBO Rep* 4: 948 – 952
35. Choi SY, Huang P, Jenkins GM, Chan DC, Schiller J, Frohman MA (2006) A common lipid links Mfn-mediated mitochondrial fusion and SNARE-regulated exocytosis. *Nat Cell Biol* 8: 1255 – 1262
36. Ma W, Kim H, Songyang Z (2011) Studying of telomeric protein-protein interactions by Bi-molecular fluorescence complementation (BiFC) and peptide array-based assays. *Methods Mol Biol* 735: 161 – 171
37. Hofmann MC, Braydich-Stolle L, Dettin L, Johnson E, Dym M (2005) Immortalization of mouse germ line stem cells. *Stem Cells* 23: 200 – 210
38. Ross JM (2011) Visualization of mitochondrial respiratory function using cytochrome c oxidase/succinate dehydrogenase (COX/SDH) double-labeling histochemistry. *J Vis Exp* 57: e3266
39. Gallardo T, Shirley L, John GB, Castrillon DH (2007) Generation of a germ cell-specific mouse transgenic Cre line, Vasa-Cre. *Genesis* 45: 413 – 417
40. Rambold AS, Kostelecky B, Elia N, Lippincott-Schwartz J (2011) Tubular network formation protects mitochondria from autophagosomal degradation during nutrient starvation. *Proc Natl Acad Sci USA* 108: 10190 – 10195
41. Sogo LF, Yaffe MP (1994) Regulation of mitochondrial morphology and inheritance by Mdm10p, a protein of the mitochondrial outer membrane. *J Cell Biol* 126: 1361 – 1373
42. McManus MT, Ma L, Buchold GM, Greenbaum MP, Roy A, Burns KH, Zhu H, Han DY, Harris RA, Coarfa C *et al* (2009) GASZ is essential for male meiosis and suppression of retrotransposon expression in the male germline. *PLoS Genet* 5: e1000635
43. Zhang J, Liu W, Liu J, Xiao W, Liu L, Jiang C, Sun X, Liu P, Zhu Y, Zhang C *et al* (2010) G-protein beta2 subunit interacts with mitofusin 1 to regulate mitochondrial fusion. *Nat Commun* 1: 101
44. Wang Y, Yates F, Naveiras O, Ernst P, Daley GQ (2005) Embryonic stem cell-derived hematopoietic stem cells. *Proc Natl Acad Sci USA* 102: 19081 – 19086
45. Gou LT, Dai P, Yang JH, Xue Y, Hu YP, Zhou Y, Kang JY, Wang X, Li H, Hua MM *et al* (2014) Pachytene piRNAs instruct massive mRNA elimination during late spermiogenesis. *Cell Res* 24: 680 – 700
46. Chen H, Vermulst M, Wang YE, Chomyn A, Prolla TA, McCaffery JM, Chan DC (2010) Mitochondrial fusion is required for mtDNA stability in skeletal muscle and tolerance of mtDNA mutations. *Cell* 141: 280 – 289

